Astron. Astrophys. 342, 709–716 (1999)

ASTRONOMY AND ASTROPHYSICS

The radio spectrum of Algol-type systems: RZ Cassiopeiae

G. Umana[1], **P. Leto**[1,4], **C. Trigilio**[1], **R.M. Hjellming**[2], **and S. Catalano**[3]

[1] Istituto di Radioastronomia del C.N.R., Stazione VLBI di Noto, C.P. 141 Noto, Italy
[2] National Radio Astronomy Observatory, Socorro, NM, USA
[3] Osservatorio Astrofisico di Catania, Viale A. Doria 6, I-95125 Catania, Italy
[4] Universitá degli studi di Messina, Dipartimento di Fisica della Materia e Tecnologie Fisiche Avanzate, Salita Sperone 31, I-98166 Messina, Italy

Received 4 March 1997 / Accepted 21 October 1998

Abstract. We present multifrequency radio observations of the Algol-type binary system RZ Cas, performed in different epochs from 1991 October to 1992 April. During this period the system shows variability in the radio flux that cannot be attributed to geometrical effects due to a partial eclipse of the radio source.

Instead, differences between radio spectra can be reproduced assuming a core-halo morphology for the radio source, where physical conditions vary as a consequence of magnetic activity. Almost simultaneous X-ray observations, carried out by other authors, allow to further constrain the physical parameters of the radio emitting region and are consistent with a co-spatial model for the X-ray and radio emitting source.

Key words: stars: activity – stars: binaries: close – stars: coronae – stars: individual: RZ Cas – radio continuum: stars

1. Introduction

Algol-type binaries are radio sources with 6 cm luminosities between 10^{15} and 10^{18} $[\mathrm{erg\ s^{-1}}]$ (Umana et al. 1991, 1998). As in the case of RS CVns, the radio emission arises from interaction of midly relativistic electrons with the magnetic field of the active secondary component and the observed radio spectra can be fitted by models of non-homogeneous gyrosynchrotron emitting plasma. In particular, Umana et al. (1993) were able to reproduce the radio spectra of some selected systems by assuming a core-halo morphology for the radio source.

RZ Cas is a bright, well-known Algol-type system, with orbital period of about 1.20 days, at a distance of 73 pcs. The system consists of an early-type primary (A3 V) and a cooler companion (K0 IV), with an orbital separation of 6.86 solar radii. The other relevant parameters of this binary system, taken from Narusawa et al. (1994), are reported in Table 1.

The system shows many peculiarities such as frequent and unpredictable period variations, which are generally interpreted in terms of mass-transfer episodes between the components (Hegedus et al. 1992), but other possible causes have been investigated (Narusawa et al., 1994). The primary minimum of the optical light-curve has been found on some occasions to resemble a partial eclipse, while on other occasions the observed flat-bottomed minimum resembles that produced by a total eclipse. Since several authors (Narusawa et al., 1994; Maxted et al., 1994) have asserted that the system is a partially eclipsing binary (i=83°.3±0°.1), this transient totality should be ascribed to other effects such as the presence of circumstellar material or to hot and cold spots on the surface of the primary component, as suggested by Olson (1982).

Table 1.

	Primary	Secondary
M [$\mathrm{M_\odot}$]	2.36	0.75
R [$\mathrm{R_\odot}$]	1.63	1.90
T [K]	8720	5150

RZ Cas is also a X-ray and radio source. In particular, Drake et al., (1986), Umana et al., (1991), Umana et al., (1993) have pointed out many analogies with the radio behavior of RS CVns, such as the high radio luminosity and the strong variability of the radio flux.

In this paper we present multi-frequency VLA observations of RZ Cas, which were obtained with the aim to investigate the origin of its radio variability. By analyzing the radio spectrum, observed at different orbital phase, it should be possible to discriminate between intrinsic source structure evolution or absorption by intersystem thermal plasma.

2. Observations and results

The observations were carried out by using the VLA[1] in different runs in the period 1991 October to 1992 April, covering different orbital phases. We observed at five frequencies, namely 1.49 (L-Band), 5.0 (C-Band), 8.4 (X-Band), 14.9 (U-Band) and 22.0 (K-Band) GHz, using two independent 50 MHz bands.

Send offprint requests to: G. Umana (umana@ira.noto.cnr.it)

[1] The Very Large Array is a facility of the National Radio Astronomy Observatory which is operated by Associated Universities, Inc. under cooperative agreement with the National Science Foundation

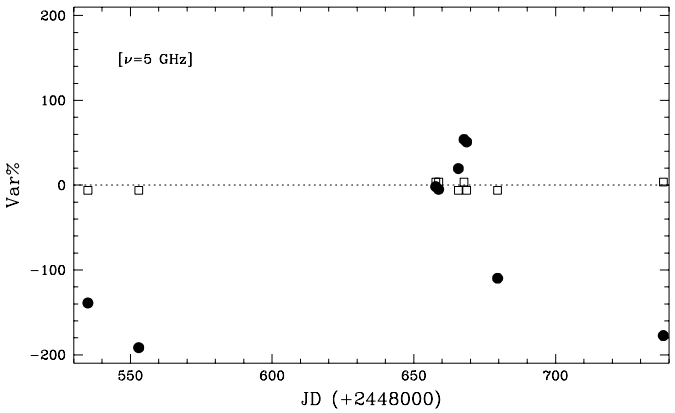

Fig. 1. Percentage variations of the 5 GHz flux density as a function of time (Julian Day) for RZ Cas and its phase calibrator. Each point represents the variations, as percentage with respect to the mean value of the radio flux density. Empty squares refer to 0224+671, while filled dots refer to RZ Cas

The observations were performed with the entire array used sequentially at each frequency. This ensures the necessary sensitivity for detection of weak sources and is suitable for sources whose variability is on timescales of an hour or longer. At each frequency a typical observing cycle consisted of 20-min integration time, preceded and followed by a 2-min observation of the phase calibrator (0224+671).

When possible, this sequence was repeated in order to improve the signal to noise ratio. The flux density scale was determined by daily observations of 3C286 and 3C48. The data were calibrated and mapped by using the standard procedures of the Astronomical Image Processing System (A.I.P.S.). We first mapped the data to find out if other sources were present in the field of view of VLA. Once problems due to possible confusion of sources were excluded, each scan was analyzed with the AIPS program DFTPL. This procedure performs the direct Fourier transform of the visibility function in a limited portion of the UV plane.

Selecting the position of the radio source, as derived from the map, it was possible to analyze the temporal behaviour of our target, with high temporal resolution and thus to locate rapid variations of the radio flux density. The results of such an analysis led to the conclusion that, even if the radio flux of RZ Cas is variable, it does not change significantly on a timescale of 20 minutes or less.

The five point spectrum was then obtained by deriving the flux density at each frequency from the cleaned map integrated over 20 min and we assume the rms of the map to be the uncertainty in the flux density. When, on the same day, two observations at each frequency were made, we derived two different values of the flux density by mapping the data relative to each scan.

Table 2 summarizes the results of these observations as follows: column 1 the date of observations, columns 2 and 3 the time of observations (UT), columns 4, 5, 6, 7 and 8 the measured radio flux density or an upper limit, with the associated rms error, at the various frequencies. Multiple values of flux density represent the results obtained by using all the data (mean value) or those for each separate scan. The measured flux densities show a large spread, but in a range consistent with previous VLA observations (Drake et al. 1986; Umana et al., 1991; Umana et al., 1993).

To exclude any spurious variations in the data of different epochs due to flux calibration, we compared the time behaviour of the radio flux of 0224+671 with that of RZ Cas at different frequencies. As an example, we plot in Fig. 1 the flux of the calibrator at 5 GHz, as percentage of the averaged value, together with radio flux of RZ Cas. It is evident that the calibrator flux did not vary within 10% while RZ Cas showed variations up to 200%. The same trend is observed in the other bands. As already pointed out, the radio emission of RZ Cas is variable at all the observed frequencies.

3. The behaviour of the radio variability

We performed the radio observations of RZ Cas over a wide time interval of about 7 months, starting on October 1991. Due to our irregular sampling, it is not easy to assess a typical time scale for the variability.

In an eclipsing binary the most obvious time scale for variability is the orbital period. We thus checked if the observed variability may be related to a geometrical effect, as the sky projection of the radio source changes as the system rotates. However, no correlation with the orbital phase is evident from our data, as one would expect in case of rotational modulation of the radio flux, assuming that the rotational period of the secondary star is synchronized to the orbital period.

Instead the radio emission seems to be characterized (see Table 2) by periods of low flux density level (0.7–1 mJy) and a high (2–3 mJy), highly variable level, that we will refer to as an active period. On previous observations RZ Cas was found at intermediate, 1.35 mJy (June, 1985) and 1.25 mJy (Feb.1989) as well as high emission levels, i. e., 3.45 mJy (Nov. 1984) (Drake et al., 1986; Umana et al., 1991).

From the flux densities, measured at each frequency and shown in fig 2, it seems that in the active period (panel b), i.e. on Feb. 1992, a flare like event has occurred around JD 2448666, i.e. in the second half of the observing period, which probably peaks between 15 and 16 February. It is interesting to note that the flux density appears to rise first at the higher frequency (K-Band) and only subsequently in the other ones. The flux enhancement appears very marginal in the L band.

Whether the high state is the result of recurrent flares, similar to those characterizing the RS CVn binaries, for example HR 1099 (Feldman et al. 1978, Umana et al. 1995) and UX Ari (Trigilio et al. 1998), it is not possible to state, because of the lack of continuous observations.

4. The origin of the radio variability

In a previous paper we have shown that the observed flat radio spectra of a sample of Algol-type binary systems cannot be

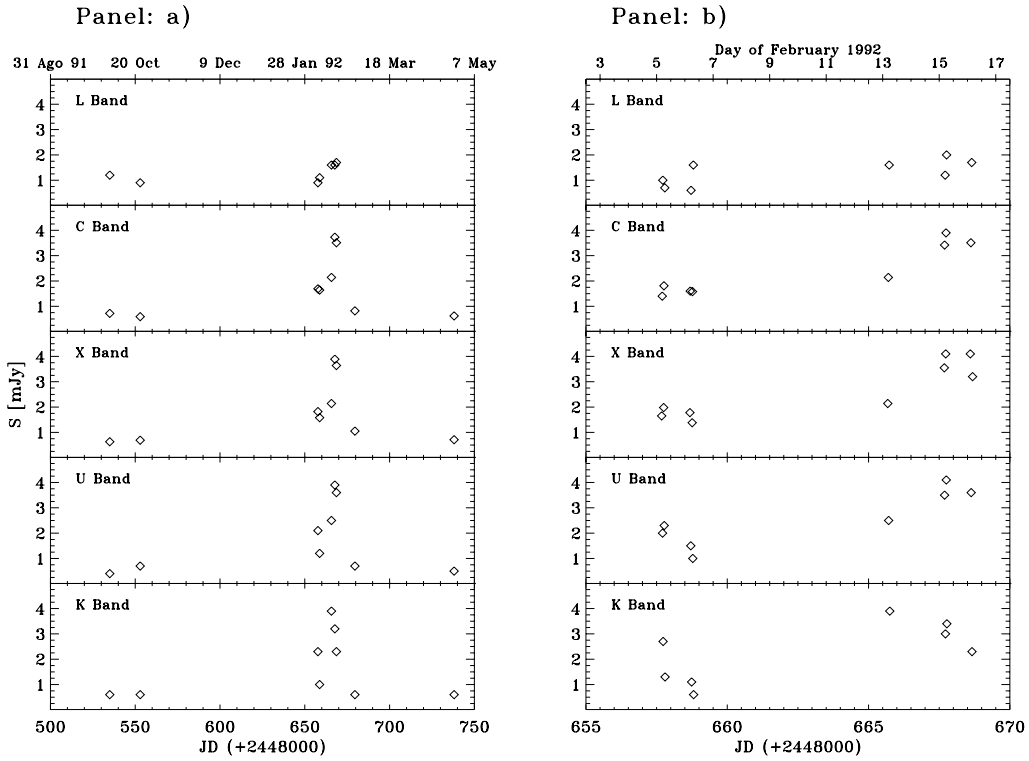

Fig. 2a and b. Flux densities observed at each frequency as functions of time (Julian Day). In panel **a** all the observations are reported, while in panel **b** the observations relative to the active period are plotted in an enlarged scale. The rms, associated to each measurement, lies well inside each square symbol.

reproduced by a homogeneous source model. We thus proposed a two component model (core-halo) to exemplify the complex morphology of the radio source (Umana et al., 1993). The closed magnetic structures of the lower corona would produce a radio source component, the *core*, characterized by high values of the magnetic field strength and size comparable to, or less then, the active stellar component.

Eventually, energetic particles in the core diffuse into higher coronal open field structures and produce a more extended tenuous radio source, the *halo*, characterized by weaker magnetic field and a lower density of energetic electrons. For their physical characteristics, the core emits mostly at higher frequencies, while the halo contributes mainly at low frequencies. The observed radio spectrum is therefore the result of these two different contributions and its shape will vary when the physical conditions of one or both components change as a consequence of, for example, flaring activity.

In our model, the core is assumed to be a compact homogeneous source with constant magnetic field (*B*) and number density ($N_{\rm rel}$), while the halo is assumed to be an extended corona with constant magnetic field and a radial dependence of the electron number density, $N_{\rm rel} = N^o_{\rm rel}(r/R_*)^{-2}$, $N^o_{\rm rel}$ being the number density at the coronal base (at R_*) and r the distance from the center of the K secondary. For both core and halo the emission and absorption coefficients have been computed assuming a power law energy distribution of the relativistic electrons, $N(E) \propto E^{-\delta}$ between $E_1 = 10$ KeV and $E_2 = 5$ MeV, with $\delta = 2$ (Umana et al. 1993).

A more rigorous model of the radio source should include a radial dependence of the magnetic field of the halo, which, for computational convenience, has instead been assumed to be constant. The core-halo morphology, where the source is sampled in two representative layers of different physical conditions, is to be assumed as a simplification of a probably very complex topology of the coronal magnetic field into two magnetic structures: small, compact loops and larger loops that have dimensions similar to the size of the entire binary system.

By applying the two component model to the RZ Cas data it is possible to determine the combination of physical parameters that best fit the observed spectra (Fig. 3).

In our previous paper (Umana et al., 1993, Fig. 3) we showed that, for a homogeneous gyrosynchrotron radio source of radius R and fixed electronic exponent distribution δ, the shape of the radio spectrum is maintained, while the frequency at which the spectrum peaks and the flux density of the peak shift toward higher values when *B*, $N_{\rm rel}$ and R increase. A functional form of these dependences can be expressed by:

$$\nu_{\rm peak} \propto B^a N^b_{\rm rel} R^c \tag{1}$$

$$S_{\rm peak} \propto B^\alpha N^\beta_{\rm rel} R^\gamma \tag{2}$$

with all the exponents a, b, c, α, β and $\gamma > 0$. Slightly different exponents can be found for a variable density distribution, as in the *halo* model, where the radius R is substituted by the thickness of the layer H. Indeed the same core or halo contributions can be reproduced by different combinations of the radius, magnetic field and energetic particle density of the emitting region.

Although is not possible to derive unique solutions, we have constrained the source parameters in small value intervals proceeding as follows. From the best fit of the observed spectra with

Table 2.

Date	UT			$S_{1.49}$ [mJy]	S_5 [mJy]	$S_{8.4}$ [mJy]	$S_{14.9}$ [mJy]	S_{22} [mJy]
	Start	End						
05 Oct 91	10:18	12:44	mean	1.2 ± 0.1	0.72 ± 0.07	0.63 ± 0.06	0.4 ± 0.1	≤ 0.6
			scan 1	1.6 ± 0.2	0.73 ± 0.07	0.66 ± 0.06	≤ 0.5	≤ 0.6
			scan 2	1.1 ± 0.2	0.66 ± 0.07	0.59 ± 0.06	≤ 0.5	≤ 0.6
23 Oct 91	09:07	12:03	mean	0.9 ± 0.1	0.59 ± 0.07	0.69 ± 0.06	0.7 ± 0.1	≤ 0.6
			scan 1	1.0 ± 0.2	0.56 ± 0.07	0.80 ± 0.06	≤ 0.6	≤ 0.6
			scan 2	0.7 ± 0.2	0.59 ± 0.07	0.66 ± 0.06	≤ 0.6	≤ 0.6
05 Feb 92	04:15	07:18	mean	0.9 ± 0.1	1.69 ± 0.07	1.82 ± 0.06	2.1 ± 0.1	2.3 ± 0.2
			scan 1	1.0 ± 0.2	1.40 ± 0.07	1.65 ± 0.06	2.0 ± 0.2	2.7 ± 0.3
			scan 2	0.7 ± 0.2	1.81 ± 0.07	1.98 ± 0.06	2.3 ± 0.2	1.3 ± 0.3
06 Feb 92	04:11	07:44	mean	1.1 ± 0.1	1.64 ± 0.06	1.58 ± 0.06	1.2 ± 0.1	1.0 ± 0.2
			scan 1	≤ 0.9	1.60 ± 0.06	1.78 ± 0.06	1.5 ± 0.1	1.1 ± 0.2
			scan 2	1.6 ± 0.3	1.58 ± 0.06	1.38 ± 0.06	1.0 ± 0.1	0.6 ± 0.2
13 Feb 92	03:48	06:14	mean	1.6 ± 0.1	2.14 ± 0.07	2.14 ± 0.06	2.5 ± 0.1	3.9 ± 0.2
15 Feb 92	04:10	06:40	mean	1.6 ± 0.1	3.73 ± 0.08	3.89 ± 0.06	3.9 ± 0.1	3.2 ± 0.2
			scan 1	1.2 ± 0.3	3.42 ± 0.08	3.55 ± 0.06	3.5 ± 0.1	3.0 ± 0.2
			scan 2	2.0 ± 0.3	3.9 ± 0.1	4.1 ± 0.1	4.1 ± 0.1	3.4 ± 0.2
16 Feb 92	02:22	07:44	mean	1.7 ± 0.1	3.51 ± 0.07	3.64 ± 0.07	3.6 ± 0.1	2.3 ± 0.2
			scan 1			4.1 ± 0.1		
			scan 2			3.20 ± 0.07		
27 Feb 92	00:06	02:12	mean		0.82 ± 0.07	1.05 ± 0.06	0.7 ± 0.1	≤ 0.6
			scan 1			1.13 ± 0.06		
			scan 2			0.94 ± 0.06		
25 Apr 92	11:58	14:34	mean		0.62 ± 0.07	0.71 ± 0.07	0.5 ± 0.1	≤ 0.6
			scan 1		0.74 ± 0.08	0.73 ± 0.07	≤ 0.6	≤ 0.6
			scan 2		0.53 ± 0.08	0.66 ± 0.07	≤ 0.6	≤ 0.6

a *core* and *halo* combination, we found the $\nu_{\rm peak}$ and $S_{\rm peak}$ for each component. Applying these values in Eqs. 1 and 2, a functional dependence of B and $N_{\rm rel}$ on R can be obtained. Thus, if we give some physical constraint on one parameter, we can derive corresponding ranges of the other ones. Among all the possible solutions we can choose a class that satisfies constraints provided by observational evidences.

Photospheric magnetic fields have recently been derived for active components of RS CVns, from the width of magnetically sensitive lines (Gondoin et al., 1985) and by means of the Zeeman-Doppler imaging technique (Donati et al. 1990; 1992). They obtained photospheric magnetic field values in the range of $B_{\rm phot} \sim 600$–$1100\,G$. Since the radio emission from Algols is very similar to that of RS CVns, and, in both cases, it is related to the magnetic activity of such systems (Umana et al., 1998), we can reasonably use similar magnetic field values for the RZ Cas models.

If we assume that the magnetosphere is mainly dipolar, we can restrict the possible range of *B* values to be those for which $B \sim B_{\rm phot}(\frac{R}{R_*})^{-3}$.

The results of the fit of various spectra are summarized in Table 3 and shown in Fig. 4 where the derived values of the magnetic field, size and energetic particles density are plotted for the halo (empty symbols) and the core (filled symbols), as a function of time. When two different spectra were obtained in the same day, a single set of physical parameters was determined, because the differences in flux densities were so small that the solution did not require any significant variation in the choice of $N_{\rm rel}$, *B* and of the source dimension.The error bar, associated with each physical parameter determination, represents the range of possible solutions that fit the spectra. In the upper part of the plots, the trend of flux density at the 8.4 GHz (X-band) is also shown. The estimated physical parameters agree very well with those derived from radio spectra of other Algol-type binaries (Umana et al., 1993).

To better appreciate how each component contributes to the observed spectra, we plot in Fig. 5 the ratio of energy emitted by the halo and the core, together with the total luminosity of RZ Cas, as inferred integrating the core-halo spectra from 0 to 40 GHz.

From Fig. 4 and Fig. 5 it appears that the physical characteristics of the two components remain almost constant during the low flux density regime. During those periods, source extension, *B* and $N_{\rm rel}$ do not show significant variations, and we can assume these values as the stationary properties of the coronal emitting regions.

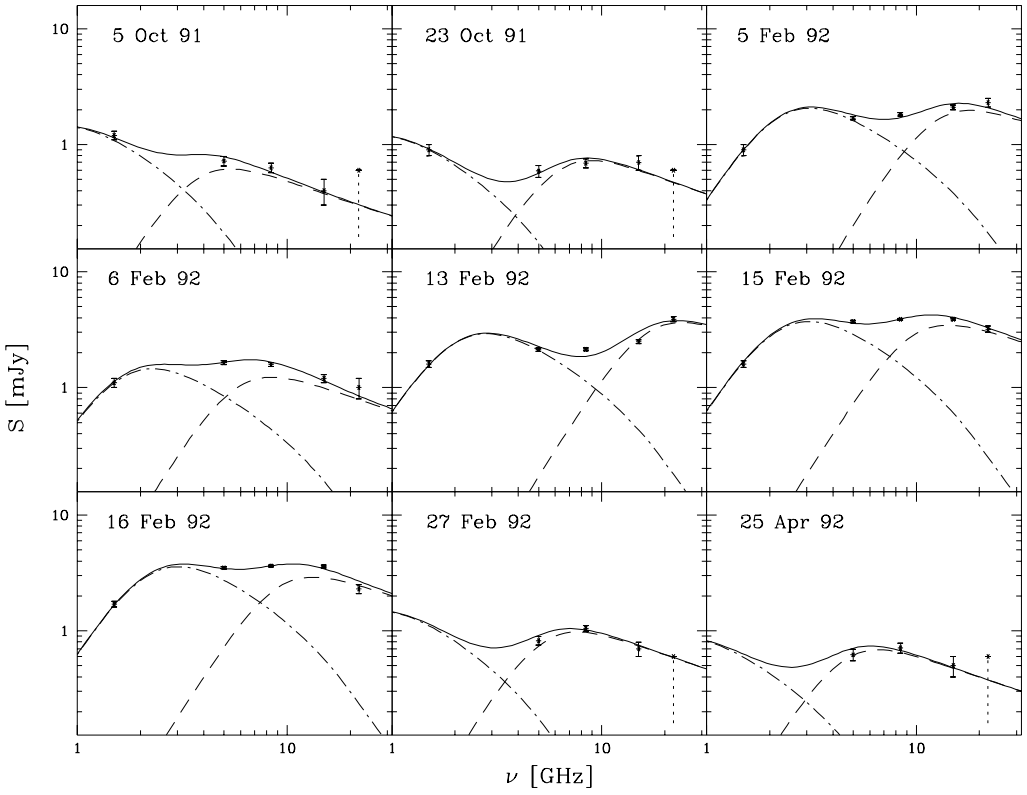

Fig. 3. Comparison between the observed radio spectra of RZ Cas and the computed spectra obtained by assuming a core-halo structure for the radio source (thick line). The contribution of the halo (dot-dashed line) and core (dashed line) to the composite spectrum are also shown

Table 3.

Date	CORE Parameters			HALO Parameters		
	B [Gauss]	Radius [R_*]	N_{rel} [$\times 10^5$ cm^{-3}]	B [Gauss]	Thickness [R_*]	N_{rel} [$\times 10^5$ cm^{-3}]
05 Oct 91	150 ± 40	0.60 ± 0.05	1.0 ± 0.5	9.5 ± 1	4.00 ± 0.25	2.0 ± 0.9
23 Oct 91	250 ± 60	0.48 ± 0.04	1.4 ± 0.8	10 ± 1	3.25 ± 0.25	1.6 ± 0.9
05 Feb 92	320 ± 90	0.35 ± 0.03	9.8 ± 6.0	65 ± 10	1.35 ± 0.15	0.6 ± 0.3
06 Feb 92	185 ± 40	0.63 ± 0.05	1.5 ± 0.8	45 ± 8	1.55 ± 0.15	0.6 ± 0.3
13 Feb 92	330 ± 100	0.34 ± 0.03	20 ± 10	46 ± 8	1.65 ± 0.15	1.3 ± 0.5
15 Feb 92	210 ± 50	0.56 ± 0.04	6.6 ± 3.5	46 ± 8	1.65 ± 0.15	1.8 ± 0.8
16 Feb 92	210 ± 50	0.56 ± 0.04	5.2 ± 3.0	45 ± 8	1.65 ± 0.15	1.7 ± 0.7
27 Feb 92	190 ± 40	0.63 ± 0.05	3.4 ± 2.0	9 ± 1	3.50 ± 0.30	3 ± 1
25 Apr 92	180 ± 40	0.64 ± 0.05	2.2 ± 1.0	10 ± 1	3.25 ± 0.25	1.2 ± 0.5

During the active period (data between dashed vertical lines in Fig. 4) the physical parameters of both the halo and core show significant changes. The magnetic field of the halo is found to considerably increase (about a factor of 6) while the effective size is apparently decreased. The contribution to the total flux becomes greater due to the combination of the increase of the magnetic field and the number density. Thus the halo seems to be characterized by more compact coronal structures, which contribute an almost equal amount as the core to the observed spectrum of the active source (Fig. 5).

The magnetic field and size of the core do not show significant changes with respect to the quiescent period, however the electron density number is increased up to a factor of ten, with large fluctuations. This is not surprising, because the core is probably the site where energetic emitting particles are produced and thus where radio flares originate. Moreover, due to its compact dimension, the core may evolve in a time scale much shorter than the more extended halo.

Probably a flare-like event occured on 13 Feb. The higher values of B and $N_{\rm rel}$ we derived for the core seem to indicate that an energy release was first localized in a very compact region. At

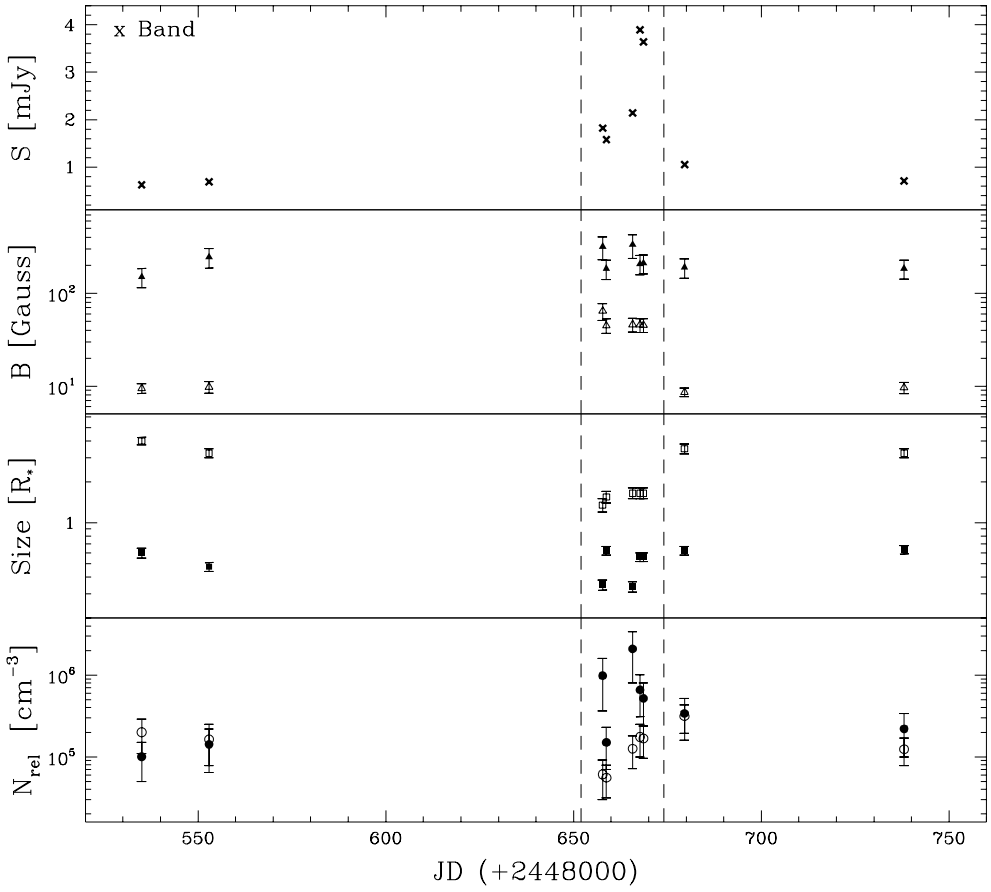

Fig. 4. Physical parameters as derived by applying the core-halo model. The empty symbols refer to the halo while the filled ones to the core. The linear size of the component is normalized to the radius (R_*) of the K component

this point, i.e. on February 15, it propagated towards external coronal layers, the halo contribution became more important, the radio flux increased at all the observation frequencies but at 22 GHz, which would be the first frequency to suffer the effects of the fading core.

5. Physical properties of the radio corona

RZ Cas was first detected in the soft X-ray range by Mc Cluskey & Kondo (1984). Recently its coronal X-ray emission has been the object of an extensive study by Singh et al. (1995), based on both ASCA and ROSAT observations. In particular they observed RZ Cas in the energy band between 0.1 and 4 KeV with the PSPC on board the ROSAT satellite, in two different epochs, on 1991 September (two scans) and on 1992 February (two scans).

These observations demonstrated that the source is highly variable in the X-ray domain, showing three different regimes of X-ray emission, that the authors define as low, mid and high state. The counts/s measured during the high state were almost a factor of six higher than those of low emission levels.

From spectral analysis of their data Singh et al. (1995) derived that the X-ray emission is consistent with the contribution of two different isothermal components, characterized by different volume emission measures (*EM*). The possibility to better fit the observed X-ray spectra with two isothermal components instead of using a continuous power-low distribution of *EM* has been pointed out in several X-ray observations of active binaries (Schmitt et al., 1990; White et al., 1994). This seems to indicate the presence of a highly structured, perhaps bimodal, corona.

The X-ray observations, performed on 1992 February 5, are almost simultaneous to our microwave spectrum, obtained just 2 hr before the first X-ray acquisition. During these observations the X-ray source was at the mid state. Since in the two X-ray scans, obtained more than 10 hrs apart, the same fluxes were observed, we may assume that the source was constant over hours and that the X-ray emission was due to optically thin gas, in near equilibrium between radiation and heating. In the following, we will therefore utilize the physical parameters, determined by Singh et al. (1995), to further constrain the structure of the radio emitting corona.

From spectral analysis of the February 5 observations Singh et al. (1995) derived for the first component $T_1 = 7.2 \times 10^6$ [K] and $EM_1 = 4.4 \times 10^{53}$ [cm^{-3}] and for the second component $T_2 = 4.6 \times 10^7$ [K] and $EM_2 = 3.8 \times 10^{53}$ [cm^{-3}]. There is still a very active debate as to whether in active binaries the bulk of high-temperature X-ray emission comes from high density, very compact loops (Schrijver et al., 1995) or is associated to large, low density coronal structures (Siarkowski et al., 1996) and there is observational evidence that supports both possibilities.

In the following, we will assume that the dimensions of the higher temperature component are bigger than those of the lower temperature component. If the X-ray and the radio sources

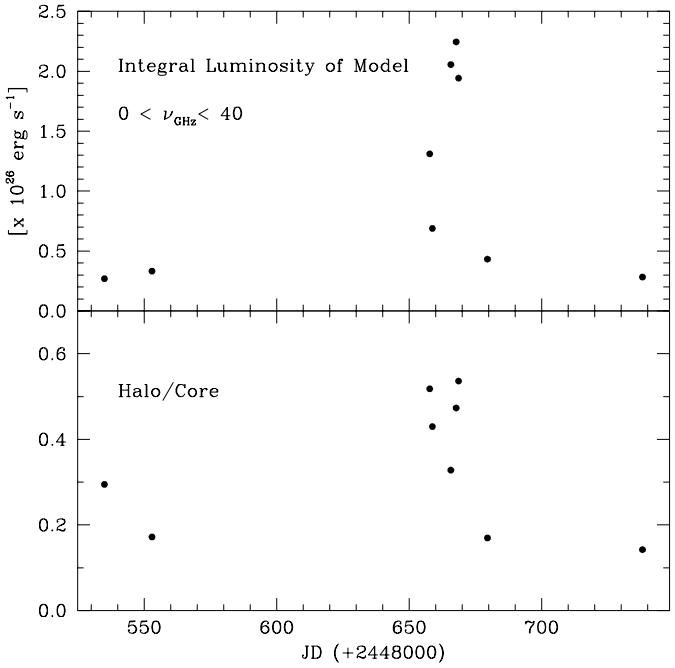

Fig. 5. *Top panel:* integrated luminosity of RZ Cas, as a function of time, in the range 0–40 GHz, from the core and halo spectra; *Bottom panel:* ratio between halo and core luminosity; The halo component contribution increases during the active regime

are co-spatial, the coronal emission regions can be separated into two separate kinds of magnetic structures: low temperature, smaller loops, which are associated with the core, and higher temperatures, larger loops, associated with the halo.

There are two principal requirements that a co-spatial model of the source must satisfy: first, the magnetic field should be able to contain the source, i.e., the density of magnetic energy should be greater than the kinetic energy of the local thermal plasma; second, the local plasma must have such a density that should not affect the radio emission by absorption.

In this scenario we can therefore derive the thermal plasma density from the X-ray data and check if the magnetic field, as determined from the radio data, can contain the X-ray source. If the plasma density is uniform in a volume V, we can write $EM = n_{\rm e}^2 V$. Thus, assuming that the X-ray emission arises from a spherically symmetric source of radius equal to the radio source we can estimate the thermal plasma density in the core and in halo, which result to be $n_{\rm e} \sim 2.9$–$3.9 \times 10^{10} [cm^{-}3]$ and $n_{\rm e} \sim 1.7$–$2.1 \times 10^{9} [cm^{-3}]$ respectively. The range of values corresponds to the possible solutions for the radius of the source (see Sect. 4).

Because the plasma must be confined by the magnetic field, the plasma β, defined as the ratio between the density of kinetic energy to the density of magnetic energy, must be less than unity. We can write β as:

$$\beta = \frac{8\pi P}{B^2} \tag{3}$$

where P represents the pressure of the thermal plasma. By replacing $2 n_{\rm e} kT$ for *P*, and using the values of magnetic field, as derived from radio observations, we will obtain $\beta = 0.009$–0.04 for the core and $\beta = 0.09$–0.26 for the halo, i. e., the magnetic pressure exceeds the gas pressure, and thus the magnetic field is strong enough that the core and halo components can be stable structures.

We consider now the possible effects that the ambient thermal plasma might have on the propagation of the radio emission. Gyrosynchrotron emission will be suppressed whenever the refractive index is significantly smaller than unity (Razin effect), i.e. at frequencies below the critical value given by:

$$\nu_{\rm R} = 20 \frac{n_{\rm e}}{B} \ [\rm Hz] \tag{4}$$

When the proper values for the core and the halo are substituted in Eq. 4, the result is that in both cases the observation frequencies are well above the critical frequency $\nu_{\rm R}$.

In conclusion, the structures assumed for the radio source are stable, i.e. using parameters consistent with the almost simultaneous X-ray observations, they can be contained by the magnetic field. Moreover, the local plasma densities, as derived from X-ray observations, assuming the source dimensions determined from our core-halo radio model, allow the propagation of the radio waves in the corona.

We reobserved the system on February 6, just 7 hours after the last X-ray observations. We found a slight difference in the high frequency part of the radio spectra, obtained in the two consecutive days, consistent with a higher contribution of the core to the resultant radio flux density. This conclusion is supported by the fact that the physical characteristic of the halo did not change between the two radio observations (see Fig. 4).

The high frequency part of the radio spectrum is strictly related to the energy content of the emitting population. Thus, a variation of the slope in this range of frequency will reflect how the energy of the relativistic electrons varies as a consequence of the energy loss mechanism operating in the radio emitting region. The different contribution of the core on February 6 can be therefore ascribed to a higher efficiency of the loss mechanism in more compact magnetic structures. However the overall observed flux density remained at a comparable level to Feb 5. If we assume as the quiescent or basal flux density of RZ Cas the level measured on 1991 Oct 5 or 1992 Apr. 25 ($\langle S_{6\ cm} \rangle \sim 0.65$ [mJy]), we may conclude that, as in the X-ray regime, in the period between Feb 5 and 6, the radio emis sion of RZ Cas showed a kind of "middle state" of energy level.

Gyrosynchrotron emitting electrons, injected in loops filled by thermal plasma of density $n_{\rm e}$, will thermalize in a time scale given by (Benz & Gold, 1971):

$$\tau_{\rm coll} = 1.6 \times 10^{12} \frac{E}{n_{\rm e}} \tag{5}$$

where E represents the electron energy expressed in MeV. This time, for electron energies in the range between 0.1–10 MeV, will be 1.2–153 minutes for the halo and 0.06–9 minutes for the core. This means that to maintain the observed mid state level for up to two days a continuous ejection of relativistic electrons in the coronal regions is necessary.

6. Conclusions

We confirm the variability of the radio flux density of the Algol-type binary system RZ Cas, that cannot be ascribed to any geometrical effects related to an eclipse of the radio source. Instead, the observed variability and the changes in the radio spectrum are consistent with a core-halo morphology of the radio emitting corona, where the physical conditions vary due to the magnetic activity.

The existence of such a structured corona is supported by almost simultaneous X-ray observations, reported in the literature, and carried out with ROSAT. The X-ray flux is, in fact, well reproduced by assuming two distinct regions of the corona, characterized by different temperature and emission measures. When physical parameters, as derived from radio spectra, are combined with those inferred from X-ray observations, a co-spatial model for the X-ray and radio source can be outlined, where the radio structures, i.e. core and halo, correspond to the two X-ray emitting regions. Finally, the quiescent radio emission of RZ Cas cannot be attributed to gyrosynchrotron from a thermal population of emitting particles, as already pointed out in a recent paper by Umana et al. (1998). Therefore, the observed quiescent flux density requires a presence of energetic nonthermal electrons in the corona, even in epochs of low level of magnetic activity. By variability timescale considerations we have shown that these energetic electrons must be supplied almost continuously, in order to maintain the observed quiescent radio component.

References

Benz A.O., Gold T., 1971, Solar Phys 21, 157
Donati J.F., Brown S.F., Semel M., et al., 1992, A&A 265, 682
Donati J.F., Semel M., Rees D.E., Taylor K., Robinson R.D., 1990, A&A 232, L1
Drake S.A., Simon T., Linsky J.L., 1986, AJ 91, 1229
Feldman P.A., Taylor A.R., Gregory P.C., et al., 1978, AJ 83, 1471
Gondoin Ph., Giampapa M.S., Bookbinder J.A., 1985, ApJ 297, 710
Hegedus T., Szatmary K., Vinko J., 1992, Ap&SS 187, 57
Maxted P.F.L., Hill G., Hilditch R.W., 1994, A&A 282, 821
Mc Cluskey G.E., Kondo Y., 1984, PASP 96, 817
Narusawa S., Nakamura Y., Yamasaky A., 1994, AJ 107, 1141
Olson E.C, 1982, ApJ 259, 702
Richards M., Albright G., 1993, AJSS 88, 199
Schmitt J.H.M.M., Collura A., Sciortino S., et al., 1990, ApJ 365, 704
Schrijver C.J., Mewe R., van den Oord G.H.J., Kaastra J.S., 1995, A&A 302, 438
Siarkowski M., Pres P., Drake S.A., White N.E., Singh K.P., 1996, ApJ 473, 470
Singh K.P., Drake S.A., White N.E., 1995, ApJ 445, 840
Swank J.H, White N.E., Holt S.S., Becker R.H., 1981, ApJ 246, 208
Trigilio C., Leto P., Umana G., 1998, A&A 329, 1060
Umana, G., Catalano, S., Rodonó, M., 1991 A&A 249, 217.
Umana G., Trigilio C., Hjellming R.M., Catalano S., 1993, A&A 267, 126
Umana G., Trigilio C., Tumino M., Catalano S., Rodonó M., 1995, A&A 298, 143
Umana G., Trigilio C., Catalano S., 1998, A&A 329, 1010
White N.E., et al., 1994, PASJ 46, L97